ChemElectroChem

Research Article
doi.org/10.1002/celc.202200272

Chemistry Europe
European Chemical Societies Publishing

www.chemelectrochem.org

Special Collection

Electrochemical Reduction of CO_2 to Formate on Nanoparticulated Bi–Sn–Sb Electrodes

Beatriz Ávila-Bolívar, Vicente Montiel, and José Solla-Gullón*[a]

Human activities during the last century have increased the concentration of greenhouse gases in Earth's atmosphere, mainly carbon dioxide (CO_2), and the impacts of climate change around the world are becoming more damaging. Therefore, scientific research is needed to mitigate the consequences of atmospheric CO_2, and, among others, the electrochemical CO_2 conversion to useful chemicals is one of the most interesting alternatives. Herein, different Bi, Sn and Sb systems were synthesised as nanoparticles, supported on carbon (Vulcan XC-72R) and finally used to manufacture electrodes. The Bi–Sn–Sb nanoparticulated systems and their corresponding electrodes were characterised by TEM, XPS, ICP-OES and SEM. Electrochemical reduction of CO_2 to formate was performed in an electrochemical H-type cell in a CO_2-saturated $KHCO_3$ and KCl solution. The Bi–Sn–Sb electrodes exhibited good activity and selectivity for the CO_2 reduction towards formate. Particularly, $Bi_{95}Sb_{05}$/C and $Bi_{80}Sn_{10}Sb_{10}$/C electrodes showed improved stability compared to previous works, keeping values of formate efficiency over 50% after 24 h.

Introduction

Atmospheric CO_2 accumulation is one of the most challenging problems for the climate change nowadays. In consequence, important advances in carbon capture, utilization and storage (CCUS) have been made over the last several decades.[1] Carbon dioxide utilization is an attractive alternative to reduce atmospheric CO_2 concentration, capable of converting CO_2 into valuable products using renewable energy sources. Different CO_2 conversion technologies have been proposed related to photochemical, electrochemical, biochemical or chemical methods.[2–4] Electrochemical routes present interesting advantages compared to other strategies because the process can occur at room temperature, scaling up is easy and generation of products selectively is possible.[5] Even though electrochemistry requires electrical energy, products obtained can be used as energy source, reducing costs.[6]

Methane, methanol, formic acid, carbon monoxide, ethanol and ethylene are the main chemicals that the electrochemical CO_2 reduction reaction (ECO_2RR) can produce. Among them, formic acid (HCOOH) is an important raw material for processing pharmaceutical and chemical products. Moreover, HCOOH is a liquid fuel for proton-exchange membrane fuel cells.[7] Due to the ability to store hydrogen in liquid form, HCOOH is one of the most economically viable products during CO_2 electroreduction process.[8] Specific catalysts are required for the selective CO_2 conversion towards HCOOH. Main group metals including Sn,[9,10] Bi,[11,12] Sb,[13,14] Cd,[15] Pb,[16] or In[17,18] are able to catalyse the reduction of CO_2 to formic acid/formate selectively. However, slow kinetics for the ECO_2RR reduce efficiency due to the conversion of H_2O to H_2. For this reason, new strategies have been taken to find more active, selective and stable electrocatalysts.

Bimetallic electrocatalysts can play an interesting role for the CO_2RR. For instance, He and co-workers published a detailed review about bimetallic mixtures and the studies showed an improvement in the performance for the CO_2 reduction due to the use of these systems.[19] More recently, works have continued this topic using Sn–Pb–Sb alloy foil,[20,21] nanoporous Cu–Ag alloys,[22] Cu–Sn alloys,[23–26] Sn–Sb alloys,[27] Cu–Sb alloys,[28] Cu–Bi amorphous bimetallic electrocatalysts,[29] or In–Sn alloy core-shell nanoparticles.[30]

Tin and bismuth are the most studied metals for the CO_2RR towards formic acid/formate and, with respect to them, recent bimetallic studies have revealed that the Bi presence improves the performance of Sn catalysts,[31,32] although pure Bi catalysts outperform those combining Sn and Bi.[33] However, this behaviour also depends on the structure. A recent study with Bi/Sn bimetallic electrocatalyst showed that an intermediate proportion of Bi and Sn exhibited the best activity.[34] In addition to Bi and Sn bimetallic studies, antimony have demonstrated to improve the activity of other metals. SnSb alloy films,[27] specifically, Sn_9Sb_1 film, showed a better behaviour than pure Sn.

In Table S1, we summarize the main characteristics of some of our previous contributions on this topic. However, it is worth noting that in all cases, long-term stability represents a major limitation that have strongly hampered the advance of these

[a] B. Ávila-Bolívar, Prof. V. Montiel, Dr. J. Solla-Gullón
Institute of Electrochemistry
University of Alicante
Apdo. 99, E-03080 Alicante, Spain
E-mail: jose.solla@ua.es

Supporting information for this article is available on the WWW under https://doi.org/10.1002/celc.202200272

Special Collection *An invited contribution to a Special Collection on Current Trends in Electrochemistry 2021 for the 1st French-Spanish Workshop on Electrochemistry*

nanomaterials as electrocatalysts for CO_2 electroreduction. In this sense, as recently discussed by Breugelmans et al. for Sn-based electrocatalysts, several degradation pathways may take place during the reaction including agglomeration, dissolution/leaching, Ostwald ripening, particle detachment, passivation/oxidation, poisoning, pulverization and reshaping.[35] Therefore, understanding the degradation pathways represents a major challenge that needs to be addressed for the implementation of this electrochemical technology in practical applications. In this regard, more recently, we used Sb/C NPs for the formate production. Despite this electrocatalyst showed, as expected, low activity, its stability under working conditions was noticeable.[14] Because of these characteristics, an understanding study of tin, bismuth and antimony combinations could be beneficial for the ECO_2RR. Consequently, in this work, carbon supported BiSn, BiSb, SnSb and BiSnSb nanoparticles were synthesised, and physicochemical and electrochemically characterised. These nanoparticles were evaluated for the electrochemical reduction of CO_2 to formate in order to find a good system with improved trade-off properties in terms of activity, selectivity and stability.

Results and Discussion

Characterization of Nanoparticles

A detailed description of the synthesis of these nanoparticles is included in the Experimental Section and Table S2. Dispersion, morphology and size of the nanoparticles were studied with transmission electron microscopy. Figures 1 and 2 show some representative transmission electron microscopy (TEM) images of the different samples. For BiSn/C samples (Figure 1), the images show a homogeneous dispersion of quasi-spherical nanoparticles, with a small tendency to agglomerate for higher proportions of Sn. As discussed in previous works,[14] antimony nanoparticles displayed a higher particle size and a larger agglomeration. Similar behaviour appears for $Bi_{80}Sb_{20}$/C, $Bi_{95}Sb_{05}$/C, $Sn_{80}Sb_{20}$/C and $Bi_{80}Sn_{10}Sb_{10}$/C samples (Figure 2).

The particle size of each sample was estimated with similar images to Figures 1 and 2, and relative frequency were calculated based on measurements of approximately 200 nanoparticles per sample. The corresponding particle size histograms are shown in Figures 3 and 4. The particle size was found to be around 10 nm for BiSn nanoparticles although a wider range of sizes is observed for increasing Sn contents (Figure 3). Thus, for instance, in $Bi_{20}Sn_{80}$/C, some particles of about 20 nm can be also observed. Figure 4 shows the particle size histograms obtained with the Sb-containing systems. In these cases, similar particle sizes, between 9 and 12 nm, have been also observed.

Inductively coupled plasma optical emission spectrometry (ICP-OES) analysis were conducted to determine the actual metal loading of the samples and Table S3 shows the obtained results. The actual metal loading was slightly lower than the nominal one (20 wt%) for every sample. This can be attributed to a residual presence of *N*,*N*-Dimethylformamide (DMF) and polyvinylpyrrolidone (PVP) trapped in the porosity of the carbon

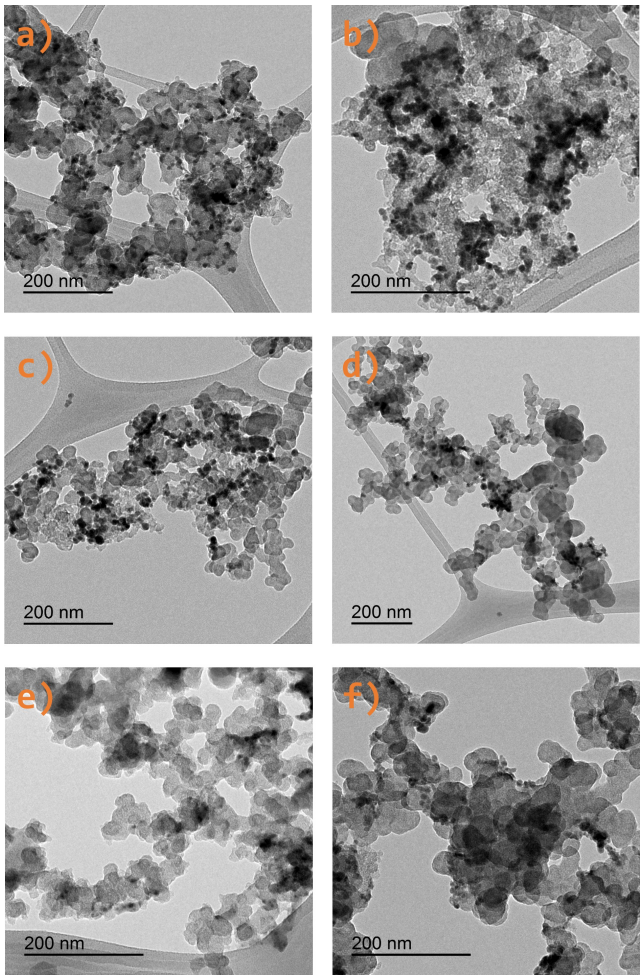

Figure 1. Representative TEM images of a) Bi/C, b) $Bi_{80}Sn_{20}$/C, c) $B_{i60}Sn_{40}$/C, d) $Bi_{40}Sn_{60}$/C, e) $Bi_{20}Sn_{80}$/C, and f) Sn/C.

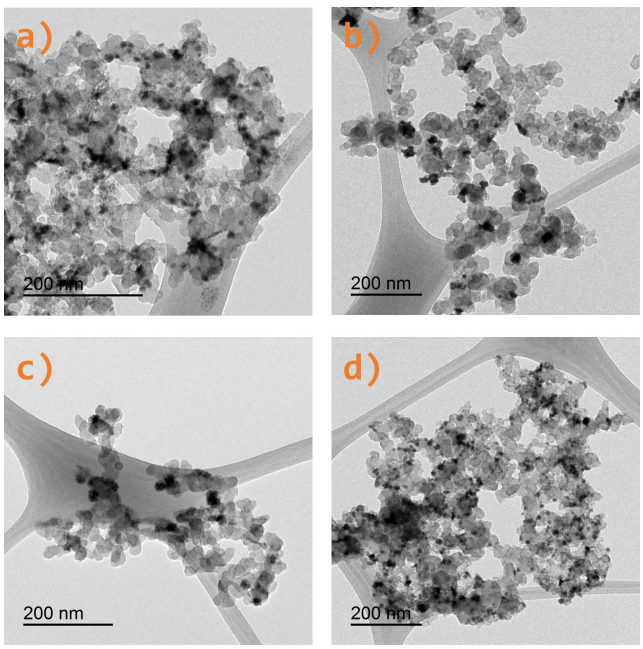

Figure 2. Representative TEM images of a) $Bi_{80}Sb_{20}$/C, b) $Bi_{95}Sb_{05}$/C, c) $Sn_{80}Sb_{20}$/C, and d) $Bi_{80}Sn_{10}Sb_{10}$/C.

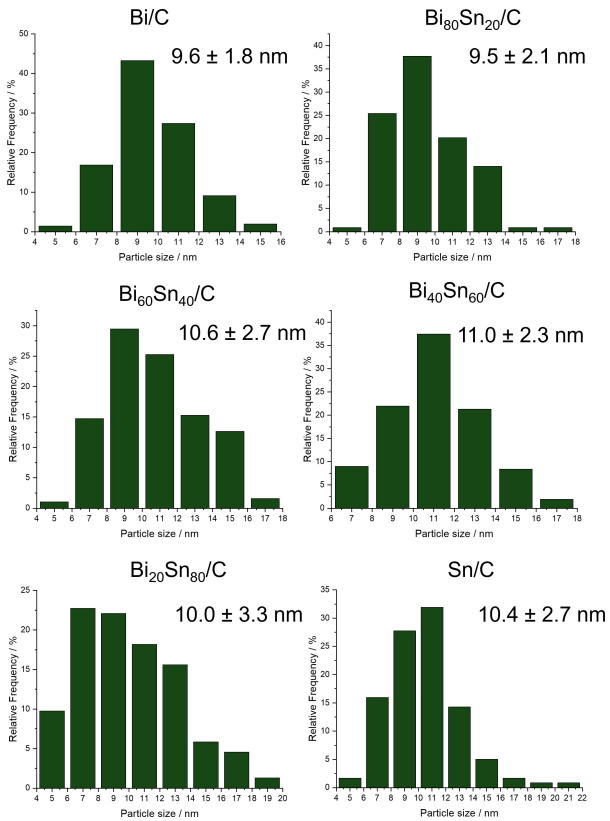

Figure 3. Particle size histogram corresponding to the BiSn-based nanoparticles.

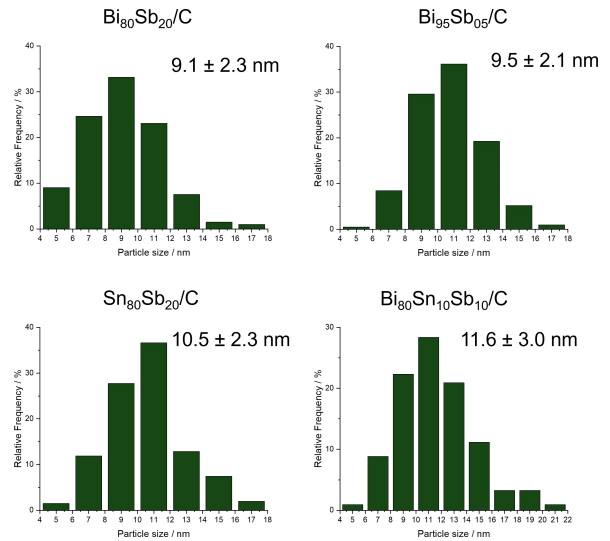

Figure 4. Particle size histogram corresponding to the Sb-containing nanoparticles.

Vulcan as well as to some partial dissolution of the metals during the extensive washing steps of the samples.

The surface composition and the oxidation states of the different elements were examined by X-ray Photoelectron Spectroscopy (XPS) measurements. Figure S1 shows Bi 4f and Sn 3d spectra of Bi/C, $Bi_{80}Sn_{20}$/C, $Bi_{60}Sn_{40}$/C, $Bi_{40}Sn_{60}$/C, $Bi_{20}Sn_{80}$/C and Sn/C samples. For the Bi/C sample, Bi 4f spectra deconvoluted into two peak groups, which correspond to Bi^{3+} at 159.6 ($4f_{7/2}$) and 164.9 eV ($4f_{5/2}$) and Bi^0 at 157.4 ($4f_{7/2}$) and 162.6 eV ($4f_{5/2}$). The spectrum of Sn 3d for Sn/C sample included Sn^0 at 486.0 and 495.1 eV, and Sn^{2+} at 487.2 and 495.6 eV. The peaks at higher binding energy correspond to Sn $3d_{3/2}$ and, the peaks at lower, to Sn $3d_{5/2}$. Integration of the Bi/C spectral signal indicated that 88% of the bismuth atoms present on the surface are oxidized, while the remaining 12% are in the Bi^0 oxidation state, and for Sn/C, the proportion is 93:7 (Sn oxides: Sn^0). In the case of BiSn/C samples, similar patterns were observed except that only metal oxides were noticeable for Bi 4f and Sn 3d. For Sn 3d, the spectrum displayed peaks at 487.0 and 495.5 eV corresponding to SnO and peaks at 488.0 and 497.1 eV associated to SnO_2, suggesting the presence of mixed oxides. These values agree with those previously observed in similar samples.[31,32,34] Figure S2 shows Bi 4f, Sn 3d and Sb 3d spectra of $Bi_{80}Sb_{20}$/C, $Bi_{95}Sb_{05}$/C, $Sn_{80}Sb_{20}$/C and $Bi_{80}Sn_{10}Sb_{10}$/C samples. Sb 3d patterns displayed two peaks at 531 ($3d_{5/2}$) and 540 ($3d_{3/2}$) eV associated to Sb_2O_3. It is noteworthy that $Bi_{95}Sb_{05}$/C sample showed a peak corresponding to metallic bismuth, the same as in the Bi/C sample. This is probably due to the higher concentration of bismuth in the sample, higher than 80%. Summarizing, XPS spectra indicated that Bi, Sn and Sb oxides can be considered as the main components of the samples. Exposed to air, the formation of oxides is a highly spontaneous reaction, and this explains the oxide predominance.[36] Nevertheless, it is very important to recall that, during the electrochemical experiments, the electrode potential will be placed at more negative potentials that those corresponding to the potential where oxides are electrochemically reduced to metallic state, and, consequently, the CO_2 reduction experiments will be performed on metallic samples. The actual atomic proportion of Bi, Sn and Sb on the surface are reported in Table S4. As general trend, the results showed a certain Sn enrichment at the surface of the nanoparticles.

Characterization of Toray-Based Electrodes

The manufactured electrodes were characterised by scanning electron microscopy (SEM) to evaluate how the catalytic inks cover the Toray paper substrates. Figures S3 and Figure S4 show some representative SEM images at different magnification also including energy dispersive X-ray (EDX) mapping of the plane section of the electrodes. SEM images indicate a homogeneous covering of the carbon supported nanoparticles on the carbon fibbers. However, some clusters are also observed, especially for the Sb samples, which is in line with a previous work.[14] The catalytic inks are deposited over the entire surface in uniform and compact layer, as can be seen in SEM-EDX images. For $Bi_{95}Sb_{05}$/C and $Bi_{80}Sn_{10}Sb_{10}$/C samples (Figure S4), the amount of Sn and Sb is too small to be detected by EDX, and for this reason, only Bi is including in the SEM-EDX mapping.

Electrochemical Characterisation

Figure 5 reports the cyclic voltammograms obtained in Ar and CO_2 saturated solutions with the BiSn-based electrodes. For sake of comparison, Bi and Sn rods were also used and electrochemically characterised under the same conditions than those employ with the bimetallic systems. The results are included in Figure S5.

The results obtained BiSn-based electrodes, in comparison with the Bi and Sn rod, display much larger double layer contributions due to the presence of the porous carbon Vulcan and the Toray-paper substrate. Previous studies demonstrated that these carbon substrates are inactive for the CO_2 reduction.[14] In Ar saturated solution, and both for the nanoparticulated electrodes and metal rods, the onset potential of the hydrogen evolution reaction (HER) takes places at about −1.5 V vs AgCl/Ag. Bi/C electrode presents an oxidation process with two peaks at −0.3 and −0.1 V vs AgCl/Ag, attributed to the superficial electrochemical oxidation of Bi to Bi_2O_3. The reduction of Bi_2O_3 to Bi appears at −0.75 V with a single peak in the negative going sweep. For Sn/C electrode, between −0.8 V and −0.6 V occurs the oxidation of metallic Sn to Sn oxides whereas at about −1.0 V, the Sn oxide electrochemical reduction to metallic Sn is clearly visible. BiSn samples displays similar features associated to the corresponding oxidation or reduction of the surfaces. Interestingly, for CO_2 saturated solutions, Bi/C, Sn/C and BiSn/C samples show an evident reduction process at about −1.4 V vs AgCl/Ag which is not present in case of Ar saturated solution and, therefore, it can be attributed to the CO_2 electrochemical reduction thus evidencing that all the nanoparticulated electrodes are actives for the electrochemical reduction of CO_2. Figure 6 shows similar experiments but, in this case, for the Sb-containing systems. As previously described, surface oxidation and reduction of the corresponding metallic oxides are clearly visible at comparable potentials. As expected, for the $Bi_{80}Sb_{20}$/C and $Bi_{95}Sb_{05}$/C samples, their cyclic voltammograms are very similar to that obtained with the Bi/C electrode due to the low Sb content. Voltametric features in the $Sn_{80}Sb_{20}$/C (in Ar saturated solution) are less clear compared to Sn/C, possibly due to the high CO_2 reduction process in this $Sn_{80}Sb_{20}$/C sample. The most interesting finding is that the incorporation of Sb does not significantly alter the electrocatalytic properties of Bi and Sn towards CO_2 electroreduction.

Electrochemical capacitance measurements were also performed to evaluate the surface area of the different electrodes (Figures S6 and S7). BiSn systems were compared to Bi/C, Sn/C, Bi rod and Sn rod. As expected, the carbon-supported nanoparticles displayed a significantly larger surface area than the metallic rods. In all cases, a well-defined linear behaviour is found as a function of the scan rate (Figure S6b). Capacitance values, normalised by the geometric area of the electrodes, were very similar among them, about 6 (Sn/C) and 10.4 (Bi/C) mF cm^{-2}. The Bi/C electrode showed the highest capacitance and, in general, values were lower for increasing proportions of Sn (Figure S6c). The response of the Sb-containing electrodes is reported in Figure S7. $Bi_{80}Sn_{10}Sb_{10}$/C, $Bi_{95}Sb_{05}$/C and Bi/C showed practically equal capacitance values, around 10 mF cm^{-2} (Figure S7c). However, Sn/C, Sb/C and $Sn_{80}Sb_{20}$/C electrodes exhibited lower capacitance values. Those samples with high proportion of bismuth exhibited the highest surface area, which

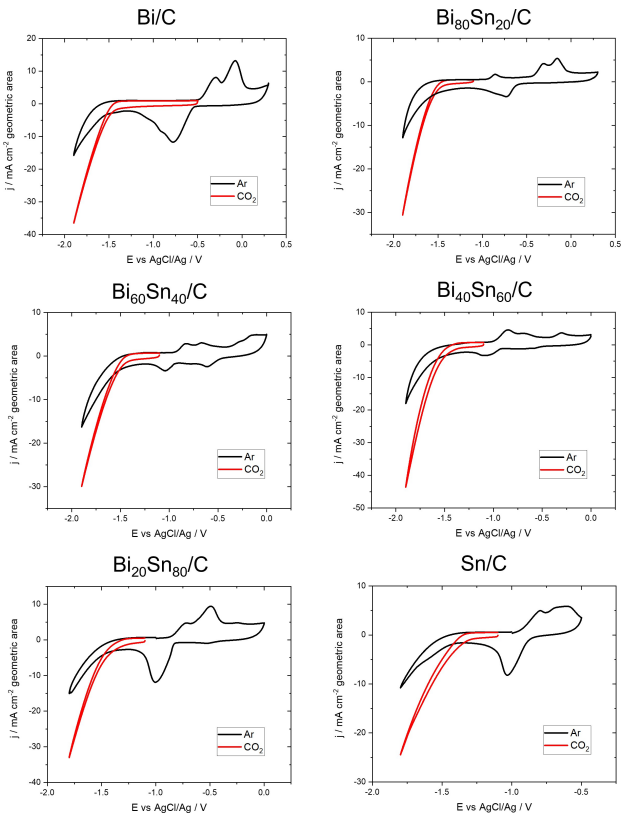

Figure 5. Cyclic voltammetry response of the BiSn/C electrodes in Ar (black line) and CO_2 (red line) saturated 0.45 M $KHCO_3$ and 0.5 M KCl solution. Scan rate 50 mV s^{-1}. Catalytic loading of 0.75 mg cm^{-2}.

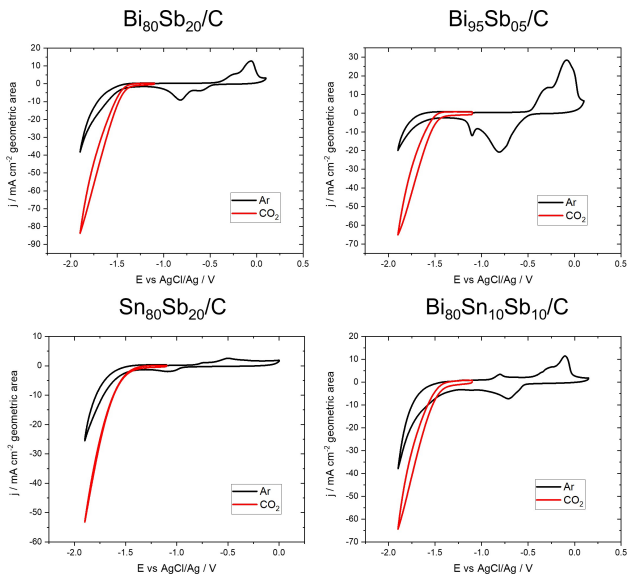

Figure 6. Cyclic voltammetry response of Sb-containing electrodes in Ar (black line) and CO_2 (red line) saturated 0.45 M $KHCO_3$ and 0.5 M KCl solution. Scan rate 50 mV s^{-1}. Catalytic loading of 0.75 mg cm^{-2}.

agrees with the capacitance results of BiSn electrodes, Figure S6. These capacitance values are in good agreement with the particle size of the nanoparticles, and, as the particle size decreases, the surface area per unit mass increases, although, obviously, the metal loading can also play a role (See Table S3).

Chronoamperometric Measurements

CO_2 electroreduction experiments were conducted in a H-type electrochemical cell in CO_2-saturated solution at −1.5, −1.6, −1.7 and −1.8 V vs AgCl/Ag. At less negative potential values than −1.5 V, the electrochemical conversion of CO_2 is almost negligible and electrolysis experiments showed the absence of products. Electrodes were freshly prepared, and the same portions of electrode was used for all the potentials. In these experiments, the electrode is firstly immersed into the solution at controlled potential of −1.1 V vs AgCl/Ag during 5 s to completely reduce the metal oxides. Then, two voltametric cycles between −1.1 V and −1.8 V were recorded at 50 mV s^{-1} to verify the status of the electrode before electrolyses. Finally, CO_2 reduction experiments were performed for 1.5 h. The results are reported in Figure 7. As observed in Figure 7, relatively stable current densities were obtained except for $Bi_{20}Sn_{80}$/C and Sn/C at −1.8 V, which displayed an evident decrease in current density over time. For Bi/C, $Bi_{80}Sn_{20}$/C, $Bi_{60}Sn_{40}$/C, and $Bi_{40}Sn_{60}$/C electrodes, currents remained essentially stable during these 6 h experiments (4 experiments of 1.5 h at different potentials). Table S5 includes a detailed analysis of the main parameters including potential, current and efficiency values for the chronoamperometric measurements obtained with the BiSn-based electrodes. The results obtained clearly evidence that for Sn-rich samples (namely Sn/C and $Bi_{20}Sn_{80}$/C), HER plays an important role on the activity and stability of the samples independently of the applied potential. However, for the rest of the samples, HER seems less evident expect at −1.8 V.

Faradaic efficiency towards formate ($FE_{formate}$) also exhibited a clear dependence on the atomic composition (Bi and Sn) of the samples. Figure 8 shows the $FE_{formate}$ as a function of the applied potential for each sample. Clearly, and independently of the nature of the sample, the $FE_{formate}$ values decrease when the applied potential is more negative. In addition, as previously indicated, this drop is more evident for Sn-rich samples (the FE of the Sn/C electrodes decreases from 56 to 12% when the applied potential changes from −1.5 to −1.8 V). This can be explained because of the exponential increase in current of the HER as well as to the lower HER overpotential on Sn than on Bi. Thus, for instance at −1.5 V, HER is almost negligible on Bi in comparison with Sn. The BiSn samples displays a performance which is in good agreement with their corresponding Bi and Sn atomic compositions. Among the samples, those with increasing proportions of Bi display improved properties, not only in terms of higher efficiencies but also less deactivation for more negative potential values. In fact, the best FE values are achieved for pure Bi/C, for which FE of about 90%, were observed at −1.5 and −1.6 V. $Bi_{80}Sn_{20}$/C and $Bi_{60}Sn_{40}$/C also displayed a good behaviour although worse than that observed for pure Bi. Thus, for instance, at −1.5 V, $Bi_{80}Sn_{20}$/C and $Bi_{60}Sn_{40}$/C showed FEs of about 80% which decrease to about 60–65% at −1.8 V. FEs for all samples and potential values are also included, Table S5.

Our findings suggest that the incorporation of Sn to Bi does not improve the efficiency and stability of the electrocatalyst and pure Bi/C electrodes exhibited the best behaviour in terms of activity and selectivity among all the BiSn tested electrodes. This observation is in agreement with previous contributions.[33]

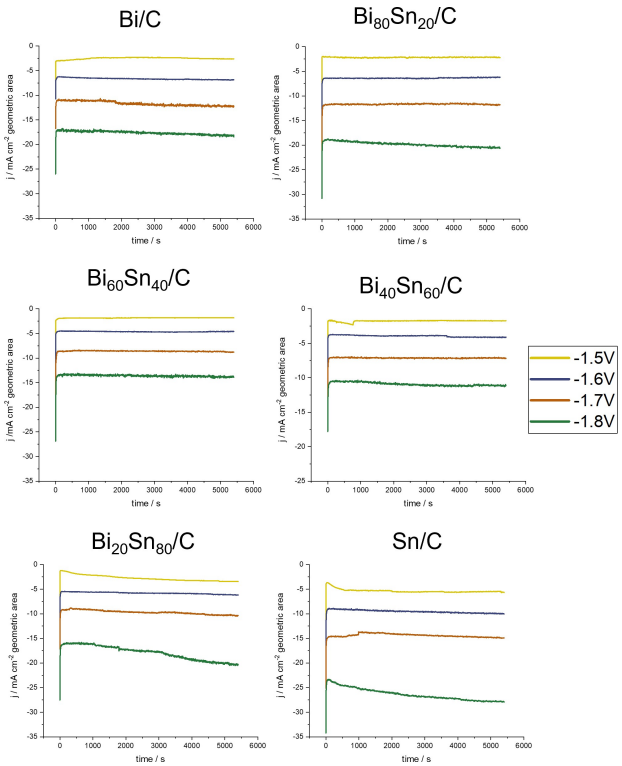

Figure 7. Chronoamperometric measurements at −1.5, −1.6, −1.7 and −1.8 V vs AgCl/Ag during 1.5 h for Bi/C, $Bi_{80}Sn_{20}$/C, $Bi_{60}Sn_{40}$/C, $Bi_{40}Sn_{60}$/C, $Bi_{20}Sn_{80}$/C and Sn/C electrodes.

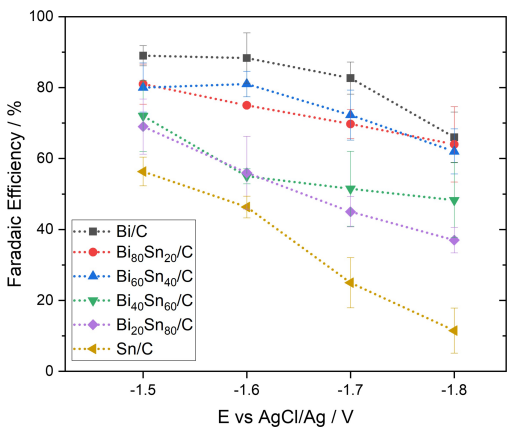

Figure 8. Faradaic efficiency of formate at relevant potentials for 1.5 h of electrolysis for Bi/C, $Bi_{80}Sn_{20}$/C, $Bi_{60}Sn_{40}$/C, $Bi_{40}Sn_{60}$/C, $Bi_{20}Sn_{80}$/C and Sn/C electrodes.

However, as previously discussed, stability is a critical issue and according with some of our previous contributions, in the case of Bi/C electrodes,[12] this is a major limitation that makes unviable their industrial implementation.

In the search of an enhanced electrocatalyst as efficient (activity and selectivity) as Bi but much more stable under working conditions, Sb-containing samples may play a role. As discussed in the introduction, and despite Sb-electrodes showed a low activity,[14] their stability was noticeable. In the following experiments, where improved stability is the main point to be considered, the electrolysis time was increased from 1.5 to 5 h. In addition, experiments were carried out at a constant potential of −1.6 V. This potential value was chosen because i) at more positive potentials, Sb was shown to be inactive for this reaction[14] and, ii) at more negative potentials, the Bi–Sn electrodes show a decay in FE (Figure 8). Figure S8 displays the variation of current density and faradaic efficiency towards formate over time for $Bi_{80}Sb_{20}$/C, $Bi_{95}Sb_{05}$/C, $Sn_{80}Sb_{20}$/C and $Bi_{80}Sn_{10}Sb_{10}$/C electrodes. For $Sn_{80}Sb_{20}$/C, current density decreased abruptly, and FE did not exceed 24%. Also, and despite the $Bi_{80}Sb_{20}$/C electrode displayed a good stability during 5 h with a constant current, $FE_{formate}$ was low, about 40% for the first hour and 30% after 5 h. In this way, these two samples, $Bi_{80}Sb_{20}$/C and $Sn_{80}Sb_{20}$/C, displayed low FE values and were discarded. Detailed values about potential, current density and formate efficiency are shown in Table S6. For the $Bi_{95}Sb_{05}$/C electrode, this exhibited the highest efficiency after 5 h within the Sb-containing electrodes (about 70%). In more details, over the first 2 hours, $FE_{formate}$ dropped considerably but them remained relatively stable at about 70%. A similar behaviour was observed with the $Bi_{80}Sn_{10}Sb_{10}$/C electrode where current and efficiency remained rather stable at about 55–60%. Based on the results obtained with the $Bi_{95}Sb_{05}$/C and $Bi_{80}Sn_{10}Sb_{10}$/C electrodes, long-term stability experiments were performed.

Figure 9 displays 24-hour electrolysis at −1.6 V vs AgCl/Ag (detailed values are included in Table S7). In these 24 h experiments, the anolyte was also analysed to evaluate a possible cross-over of formate. The results indicated the absence of formate in the anolyte. Also, the pH of catholyte was measured, showing a slightly variation from 8.4 (at the beginning of the experiment) to 8.9 (after 24 h). This small difference indicates that the pH remains essentially constant during the whole experiments. Current variation over time was very similar in both electrodes. The faradic efficiency in $Bi_{95}Sb_{05}$/C varied from 86% to 56%, (this 56% represents the best efficiency value after 24 h). However, in $Bi_{80}Sn_{10}Sb_{10}$/C, efficiency changed from 63% to 45%. In this worth noting that despite $Bi_{80}Sn_{10}Sb_{10}$/C electrode displayed lower efficiency values than $Bi_{95}Sb_{05}$/C, the drop between the first and last hour was less abrupt, that is, efficiency values were more stable than in $Bi_{95}Sb_{05}$/C. To better visualize the stability of these two samples, Figure 10 shows a stability comparison among previous and representative studies on Bi/C and Sb/C electrode. For the Bi/C electrode an evident degradation is observed after 6 hours of experiment and $FE_{formate}$ decreased to only 20% after 24 h.[12] On the other hand, despite the Sb/C electrode showed a much better stability, its $FE_{formate}$ remained at about only 15% during 24 h.[14] Under similar experimental conditions, $Bi_{95}Sb_{05}$/C and $Bi_{80}Sn_{10}Sb_{10}$/C electrodes showed a much better stability behaviour with respect to Bi/C, both in terms of current density values and $FE_{formate}$. These finding clearly indicate that the $Bi_{95}Sb_{05}$/C and $Bi_{80}Sn_{10}Sb_{10}$/C electrodes displayed an improved balance between current stability and efficiency values over time (24 h experiments). These results show that the incorporation of small quantities of Sb and Sn to Bi electrodes significantly improved its stability under electrochemical working conditions. This finding is in line with recent studies about the manipulation of the electronic and geometric structures of interfacial sites for the design of advance electrocatalysts for CO_2 electroreduction.[37–39] On the one hand, it is evident that the improvement in stability also carries a certain decrease in activity for CO_2RR. For Bi nanoparticles, electrochemical degradation becomes evident after 7–8 working hours (at −1.6 V vs AgCl/Ag). However, in case of $Bi_{95}Sb_{05}$ and $Bi_{80}Sn_{10}Sb_{10}$, the evolution of the current is much smoother which suggests that the degradation pathway is different to that observed for Bi nanoparticles. However, it is also worth noting that the reasons which the incorporation of Sb improves the stability of the samples are still unknown. In this sense, as previously mentioned in the introduction section, for Sn-based electrocatalysts, several degradation pathways may take place during the reaction including agglomeration, dissolution/leaching, Ostwald ripening, and particle detachment, among others.[35] Consequently, it would be first required to understand the main

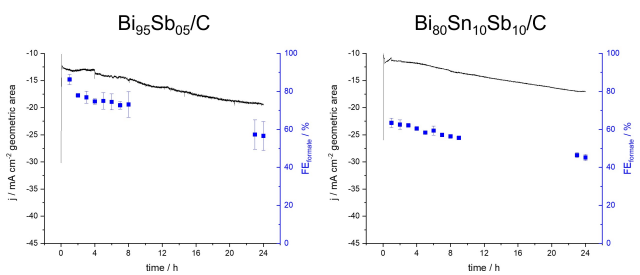

Figure 9. Long-term chronoamperometric measurements and formate faradaic efficiency over time (24 h) at −1.6 V vs AgCl/Ag for $Bi_{95}Sb_{05}$/C and $Bi_{80}Sn_{10}Sb_{10}$/C electrodes.

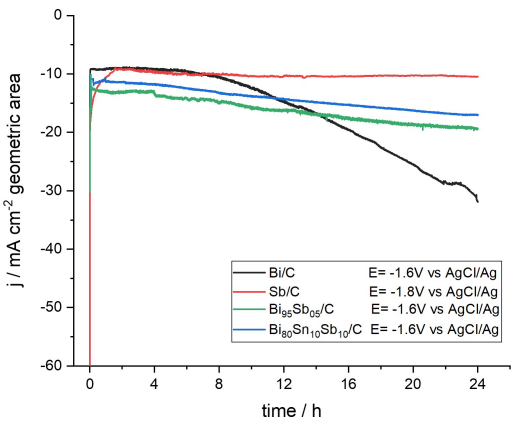

Figure 10. Comparison of long-term experiments (24 h) for Bi/C,[12] Sb/C,[14] $Bi_{95}Sb_{05}$/C and $Bi_{80}Sn_{10}Sb_{10}$/C electrodes.

mechanisms for which Bi samples degrade. This would be very valuable information to subsequently understand the origin of the stability improvement due to the incorporation of small quantities of Sb into the Bi samples. In this sense, in situ studies including in situ electrochemical transmission electron microscopy[40] and/or quasi-in-situ XPS measurements[41] can significantly contribute to properly study these degradation processes and shed light into the reasons which Sb improves the stability under electrochemical working conditions.

In addition, it is worth mention that more work is currently in progress to evaluate and verify the improved stability of these samples ($Bi_{95}Sb_{05}$/C and $Bi_{80}Sn_{10}Sb_{10}$/C electrodes) under more practical conditions, that is, in a gas phase electrochemical system[40] where only humidified CO_2 (without catholyte) and gas diffusion electrodes (GDEs) are used. This configuration has allowed not only to significantly improved efficiency and productivity values (using Bi/C electrodes) but also obtaining high concentrations of formate (higher than 300 $g \cdot L^{-1}$), thus avoiding subsequent purification costs of the product.[40]

Conclusion

In this work, carbon-supported Bi–Sn–Sb nanoparticles (about 10 nm) were synthesized using a simple, fast and scalable approach performed under room conditions. The different electrocatalysts were physicochemically characterized (TEM, XPS and ICP-OES) and used to manufacture electrodes. These electrodes were electrochemically characterized and employed for the electrocatalytic reduction of CO_2 to formate. The results indicate that for BiSn electrodes exhibited high activity for the ECO_2RR and good selective towards formate. Among them, pure Bi/C displayed the most interesting properties in terms of activity and selectivity although stability issues compromise its use. Regarding stability limitations, Sb-containing samples have shown improved performances and $Bi_{95}Sb_{05}$/C and $Bi_{80}Sn_{10}Sb_{10}$/C electrodes displayed enhanced stability. $Bi_{80}Sn_{10}Sb_{10}$/C showed essentially constant current during 24 h and reasonably stable faradaic efficiencies (from 63% to 45%). Interestingly, $Bi_{95}Sb_{05}$/C exhibited the highest faradaic efficiency to formate after 24 h (56%). These findings point out that the incorporation of small quantities of Sb (and Sn) to Bi remarkably improves its stability without significantly affecting its activity and selectivity. However, the degradation pathways for which Bi samples degrade as well as the reasons which the incorporation of Sb improves the stability of the samples are still unknown. Finally, it is worth noting that this improvement of the stability under operando conditions must be subsequently evaluated in more practical systems in which humidified CO_2 streams and GDEs are used.

Experimental Section

Chemicals and Reagents

For the nanoparticle synthesis, $BiCl_3$ (99.99%, Aldrich), $SnCl_2 \cdot 2H_2O$ (98%, Aldrich), and $SbCl_3$ (99.9%, Alfa Aesar) were used as Bi, Sn and Sb precursors, respectively. *N*,*N*-Dimethylformamide (DMF, 99.8%, Sigma Aldrich) was the solvent, polyvinylpyrrolidone (PVP, K30, Mw 55.000, Aldrich) was the capping agent, and sodium borohydride ($NaBH_4$ 99%, Aldrich) was used as reducing agent. Carbon powder (Vulcan XC-72, Cabot Corporation) was the support material. $KHCO_3$ (99.7%, Sigma Aldrich), KCl (99.5%, Emsure) were used for the catholyte solution and the anolyte was a KOH (85%, Panreac) solution. Ion exchange cross-linked resin Nafion solution (perfluorosulfonic acid - PTFE copolymer 5% w/w in isopropyl/water solution, Alfa Aesar) and ethanol absolute (VWR Chemicals) were used for the catalytic ink. Cationic ion exchange membrane Nafion 112 (DuPont) was used as separator in the electrochemical cell. A Millipore Milli-Q lab water system was employed to produce ultrapure water (18.2 MΩ cm).

Synthesis of Nanoparticles

In this work, different carbon-supported nanoparticles Bi–Sn, Bi–Sb, Sn–Sb and Bi–Sn–Sb were prepared. In particular, Bi/C, $Bi_{80}Sn_{20}$/C, $Bi_{60}Sn_{40}$/C, $Bi_{40}Sn_{60}$/C, $Bi_{20}Sn_{80}$/C and Sn/C samples were initially prepared properly to compare the activity, selectivity and stability of this Bi–Sn system. Subsequently, $Bi_{80}Sb_{20}$/C, $Bi_{95}Sb_{05}$/C, $Sn_{80}Sb_{20}$/C and $Bi_{80}Sn_{10}Sb_{10}$/C were also prepared. In all these cases, the amount of Sb was intentionally kept low. All these pure, bimetallic and trimetallic nanoparticles were synthesised using a methodology described in some of our previous contributions.[12,14,41] The synthesis of the different nanoparticles is performed at ambient temperature-pressure conditions. Firstly, the corresponding precursors are dissolved in DMF using magnetic stirring. When the solids are totally dissolved, PVP is incorporated and stirred. Then, $NaBH_4$ is added, observing a drastic colour change, from transparent to dark, indicating the reduction of M^{x+} to M^0. The mixture was stirred for 30 min with magnetic stirring and every 10 min, with ultrasound stirring. Vulcan XC-72R carbon powder was aggregated to obtain carbon supported nanoparticles, and magnetic and ultrasound stirring was used again for the complete dissolution. The metal loading of the nanoparticles, respect to the carbon support, was about 20 wt%. Acetone (nearly 5 times the volume of the sample) was added for the precipitation of the nanoparticles and this was repeated several times. For complete cleaning of samples, they were filtered through a filter funnel (POBEL) of porosity grade 4 (20 ~ 25 μm), and washed with an acetone:water (90:10) mixture. Finally, the nanoparticles were dried in an oven at 55 °C for 12 h under vacuum conditions. The specific amounts of reagents for the synthesis of the different nanoparticles are showed in Table S2.

Preparation of Cathodes

Electrodes were manufactured by spraying a catalytic ink by using an air brushing technique. The catalytic ink was prepared with metal nanoparticles, Nafion solution as binder at a catalyst:Nafion mass ratio of 80:20, and then diluted to 2 wt% in absolute ethanol. The solution was stirred by sonication for 30 min at least. The ink was directly sprayed onto a carbon paper (TGPH-90, QuinTech). To obtain uniform layers, a fast evaporation of the solvent (ethanol) is required. Therefore, the carbon paper is placed on a hot metallic plate at 90 °C. A catalytic loading of 0.75 mg NPs/C cm^{-2} were deposited for a better comparison with similar works.[12,14,40] The catalytic area of the electrodes was 9 cm^2, although approximately

4 cm^2 portions were used during the chronoamperometric measurements. The current density was normalized to this geometric area.

Physicochemical Characterisation

TEM was used to analyse the dispersion, morphology and particle size of the nanoparticles. The samples were deposited on Formvar-free lacy carbon copper grids and the TEM images were obtained at 120 kV with a JEOL JEM- 1400 Plus microscope at different magnifications. Samples were examined by using the Thermo Scientific K-Alpha X-ray Photoelectron Spectrometer (XPS). The technique is a monochromatic system (by a twin crystal monochromator) that use an Al K-alpha radiation (1486.6 eV), and a focused X-ray spot with a diameter of 400 μm at 3 mA × 12 kV. The metal loading of the carbon-supported nanoparticles was estimated by ICP-OES analysis using a Perkin Elmer Optima 4300 D system. Bi NPs were dissolved in 65 % nitric acid, and Sn and Sb NPs, in 37 % hydrochloric acid. Then, the solutions were diluted to 2 wt % HNO_3 or HCl water solution and filtered with 0,45 μm Syringe Filters. SEM (S-3000 N microscope, Hitachi) working at 20 kV was employed to analyse the catalytic layer onto the carbon support. This microscope has a Bruker brand XFlash 3001 X-ray detector for microanalysis (EDX) and mapping.

Electrochemical Characterisation

Cyclic voltammetry (CV) measurements and capacitance studies were performed in a glass cell with a three-electrode configuration. The electrolyte was Ar or CO_2-saturated 0.45 M $KHCO_3$ and 0.5 M KCl solution and a platinum wire as counter and an AgCl/Ag (3.5 M KCl) as reference electrode were used, respectively. These experiments were carried out using a PGSTAT302 N system (Metrohm Autolab B. V.) at ambient temperature. To obtain current densities, currents from every experiment were normalised by the catalytic geometric area of the electrodes (4 cm^2). A Bi rod (bismuth rod, 11 mm diameter, 99.99 % (metals basis), Alfa Aesar) and a Sn rod (tin rod, diameter 2 mm, 99.75 % purity, Goodfellow) were employed for the capacitance comparison. CO_2 electroreduction electrolyses (also using a PGSTAT302N system) were performed at controlled potentials in an H-type electrochemical cell divided by a Nafion 112 cationic ion exchange membrane. The membrane was previously activated in 0.5 M KOH for 24 h and then washed 5 h in water. A CO_2 saturated 0.45 M $KHCO_3$ and 0.5 M KCl solution was used as catholyte. A continuous CO_2 flux (200 mL min^{-1}) was maintained during the experiments. A 1.0 M KOH solution was used as anolyte. The counter electrode was a nickel mesh. An AgCl/Ag (3.5 M KCl) electrode immersed in the catholyte was used as reference electrode.

Analytical Measurements

Formate concentration was determined by ionic chromatography (883 Basic IC plus, Metrohm) with a conductivity range of 15,000 μS cm^{-1}. A 1.8 mM Na_2CO_3 and 1.7 Mm $NaHCO_3$ solution was used as mobile phase. Different calibration curves were performed depending on the electrode used, in general, from 0 to 50 ppm. The samples were diluted 100 times in water before being analysed.

Acknowledgements

This research was funded by the MICINN Spanish Ministry, through the projects CTQ2016-76231-C2-2-R (AEI/FEDER, UE) and PID2019-108136RB-C32.

Conflict of Interest

The authors declare no conflict of interest.

Data Availability Statement

The data that support the findings of this study are available from the corresponding author upon reasonable request.

Keywords: antimony · bismuth · CO_2 electroreduction · nanoparticles · tin

[1] I. Ghiat, T. Al-Ansari, *J. CO2 Util.* **2021**, *45*, 101432.
[2] F. M. Baena-Moreno, M. Rodríguez-Galán, F. Vega, B. Alonso-Fariñas, L. F. Vilches Arenas, B. Navarrete, *Energy Sources A* **2019**, *41*, 1403–1433.
[3] P. R. Yaashikaa, P. S. Kumar, S. J. Varjani, A. Saravanan, *J. CO2 Util.* **2019**, *33*, 131–147.
[4] Z. Zhang, S.-Y. Pan, H. Li, J. Cai, A. G. Olabi, E. J. Anthony, V. Manovic, *Renewable Sustainable Energy Rev.* **2020**, *125*, 109799.
[5] Q. Lu, F. Jiao, *Nano Energy* **2016**, *29*, 439–456.
[6] M.-Y. Lee, K. T. Park, W. Lee, H. Lim, Y. Kwon, S. Kang, *Crit. Rev. Environ. Sci. Technol.* **2020**, *50*, 769–815.
[7] I. Dutta, S. Chatterjee, H. Cheng, R. K. Parsapur, Z. Liu, Z. Li, E. Ye, H. Kawanami, J. S. C. Low, Z. Lai, X. J. Loh, K.-W. Huang, *Adv. Energy Mater.* **2022**, 2103799.
[8] P. Duarah, D. Haldar, V. S. K. Yadav, M. K. Purkait, *J. Environ. Chem. Eng.* **2021**, *9*, 106394.
[9] C. Zhao, J. Wang, *Chem. Eng. J.* **2016**, *293*, 161–170.
[10] A. Del Castillo, M. Alvarez-Guerra, J. Solla-Gullón, A. Sáez, V. Montiel, A. Irabien, *J. CO2 Util.* **2017**, *18*, 222–228.
[11] H. Zhang, Y. Ma, F. Quan, J. Huang, F. Jia, L. Zhang, *Electrochem. Commun.* **2014**, *46*, 63–66.
[12] B. Ávila-Bolívar, L. García-Cruz, V. Montiel, J. Solla-Gullón, *Molecules* **2019**, *24*, 2032.
[13] Z. Jiang, T. Wang, J. Pei, H. Shang, D. Zhou, H. Li, J. Dong, Y. Wang, R. Cao, Z. Zhuang, W. Chen, D. Wang, J. Zhang, Y. Li, *Energy Environ. Sci.* **2020**, *13*, 2856–2863.
[14] B. Ávila-Bolívar, V. Montiel, J. Solla-Gullón, *J. Electroanal. Chem.* **2021**, *895*, 115440.
[15] Z. Chen, N. Wang, S. Yao, L. Liu, *J. CO2 Util.* **2017**, *22*, 191–196.
[16] J. García, C. Jiménez, F. Martínez, R. Camarillo, J. Rincón, *J. Catal.* **2018**, *367*, 72–80.
[17] K. Mou, Z. Chen, S. Yao, L. Liu, *Electrochim. Acta* **2018**, *289*, 65–71.
[18] Z. Xia, M. Freeman, D. Zhang, B. Yang, L. Lei, Z. Li, Y. Hou, *ChemElectroChem* **2018**, *5*, 253–259.
[19] J. He, N. J. J. Johnson, A. Huang, C. P. Berlinguette, *ChemSusChem* **2018**, *11*, 48–57.
[20] S. Rasul, A. Pugnant, E. Yu, *ECS Trans.* **2018**, *85*, 57–66.
[21] S. Rasul, A. Pugnant, H. Xiang, J.-M. Fontmorin, E. H. Yu, *J. CO2 Util.* **2019**, *32*, 1–10.
[22] T. T. H. Hoang, S. Verma, S. Ma, T. T. Fister, J. Timoshenko, A. I. Frenkel, P. J. A. Kenis, A. A. Gewirth, *J. Am. Chem. Soc.* **2018**, *140*, 5791–5797.
[23] X. Jiang, X. Wang, Z. Liu, Q. Wang, X. Xiao, H. Pan, M. Li, J. Wang, Y. Shao, Z. Peng, Y. Shen, M. Wang, *Appl. Catal. B* **2019**, *259*, 118040.
[24] R. L. Sacci, S. Velardo, L. Xiong, D. A. Lutterman, J. Rosenthal, *Energies* **2019**, *12*, 3132.
[25] K. Ye, A. Cao, J. Shao, G. Wang, R. Si, N. Ta, J. Xiao, G. Wang, *Sci. Bull.* **2020**, *65*, 711–719.

[26] B. Ning, W. Chang, M. Liu, H. Jiang, C. Li, *ChemElectroChem* **2021**, *8*, 1150–1155.
[27] F. W. S. Lucas, F. H. B. Lima, *ChemElectroChem* **2020**, *7*, 3733–3742.
[28] S. Jia, Q. Zhu, H. Wu, M. Chu, S. Han, R. Feng, J. Tu, J. Zhai, B. Han, *Chin. J. Catal.* **2020**, *41*, 1091–1098.
[29] Y. Xiong, B. Wei, M. Wu, B. Hu, F. Zhu, J. Hao, W. Shi, *J. CO2 Util.* **2021**, *51*, 101621.
[30] J. Wang, S. Ning, M. Luo, D. Xiang, W. Chen, X. Kang, Z. Jiang, S. Chen, *Appl. Catal. B* **2021**, *288*, 119979.
[31] X. An, S. Li, A. Yoshida, T. Yu, Z. Wang, X. Hao, A. Abudula, G. Guan, *ACS Appl. Mater. Interfaces* **2019**, *11*, 42114–42122.
[32] J. Tian, R. Wang, M. Shen, X. Ma, H. Yao, Z. Hua, L. Zhang, *ChemSusChem* **2021**, *14*, 2247–2254.
[33] Q. Li, Y. Zhang, X. Zhang, H. Wang, Q. Li, J. Sheng, J. Yi, Y. Liu, J. Zhang, *Ind. Eng. Chem. Res.* **2020**, *59*, 6806–6814.
[34] Z. Li, Y. Feng, Y. Li, X. Chen, N. Li, W. He, J. Liu, *Chem. Eng. J.* **2022**, *428*, 130901.
[35] K. Van Daele, B. De Mot, M. Pupo, N. Daems, D. Pant, R. Kortlever, T. Breugelmans, *ACS Energy Lett.* **2021**, *6*, 4317–4327.
[36] E. Sutter, F. Ivars-Barcelo, P. Sutter, *Part. Part. Syst. Charact.* **2014**, *31*, 879–885.
[37] X. Shen, X. Liu, S. Wang, T. Chen, W. Zhang, L. Cao, T. Ding, Y. Lin, D. Liu, L. Wang, W. Zhang, T. Yao, *Nano Lett.* **2021**, *21*, 686–692.
[38] Y. Li, B. Wei, M. Zhu, J. Chen, Q. Jiang, B. Yang, Y. Hou, L. Lei, Z. Li, R. Zhang, Y. Lu, *Adv. Mater.* **2021**, *33*, 2102212.
[39] W. Xie, H. Li, G. Cui, J. Li, Y. Song, S. Li, X. Zhang, J. Y. Lee, M. Shao, M. Wei, *Angew. Chem. Int. Ed.* **2021**, *60*, 7382–7388.
[40] G. Díaz-Sainz, M. Alvarez-Guerra, B. Ávila-Bolívar, J. Solla-Gullón, V. Montiel, A. Irabien, *Chem. Eng. J.* **2021**, *405*, 126965.
[41] I. Sanjuán, L. García-Cruz, J. Solla-Gullón, E. Expósito, V. Montiel, *Electrochim. Acta* **2020**, *340*, 135914.
[42] R. M. Arán-Ais, R. Rizo, P. Grosse, G. Algara-Siller, K. Dembélé, M. Plodinec, T. Lunkenbein, S. Wee Chee, B. Roldan Cuenya, *Nat. Commun.* **2020**, *11*, 1–8.
[43] R. M. Arán-Ais, F. Scholten, S. Kunze, R. Rizo, B. Roldan Cuenya, *Nat. Energy* **2020**, *5*, 317–325.

Manuscript received: March 11, 2022
Accepted manuscript online: March 29, 2022